Agricultural Water Management 183 (2017) 49–59

Contents lists available at ScienceDirect

Agricultural Water Management

journal homepage: www.elsevier.com/locate/agwat

High-resolution UAV-based thermal imaging to estimate the instantaneous and seasonal variability of plant water status within a vineyard

L.G. Santesteban[a,*], S.F. Di Gennaro[b], A. Herrero-Langreo[c], C. Miranda[a], J.B. Royo[a], A. Matese[b]

[a] Dpto. Producción Agraria, Universidad Pública de Navarra, Campus Arrosadia, 31006, Pamplona, Navarra, Spain
[b] Institute of Biometeorology, National Research Council (IBIMET-CNR), Florence, Italy
[c] UMR-ITAP, Irstea. 361 rue Jean-François Breton BP 5095, 34196 Montpellier, France

ARTICLE INFO

Article history:
Received 31 May 2016
Received in revised form 11 August 2016
Accepted 24 August 2016
Available online 3 September 2016

Keywords:
Crop Water Stress Index
UAV
Stomatal conductance
Water potential
Vitis vinifera L.

ABSTRACT

Thermal imaging can become a readily usable tool for crop agricultural water management, since it allows a quick determination of canopy surface temperature that, as linked to transpiration, can give an idea of crop water status. In the last years, the resolution of thermal imaging systems has increased and its weight decreased, fostering their implementation on Unmanned Aerial Vehicles (UAV) for civil and agricultural engineering purposes. This approach would overcome most of the limitations of *on site* thermal imaging, allowing mapping plant water status at either field or farm scale, taking thus into account the naturally existing or artificially induced variability at those scales. The aim of this work was to evaluate to which extent high-resolution thermal imaging allows evaluating the instantaneous and seasonal variability of water status within a vineyard. The novelty and significance of our approach is that the specifically designed and build unmanned aerial vehicle (UAV) provided very high-resolution imaging (pixel <9 cm), and that it was used at a commercially relevant acreage (7.5 ha). This set-up was used to obtain Crop Water Stress Index (CWSI) from thermal images in a clear-sky day. CWSI values were and compared to stem water potential (Ψs) and stomatal conductance (g_s) measured at 14 sampling sites across the vineyard at the moment when images where acquired. In order to evaluate the potential of CWSI acquired in a single day to estimate within-vineyard patterns of variation in water status, a spatial modeling approach was used. CWSI correlated well with Ψs and g_s at the moment of image acquisition, showing to have a great potential to monitor instantaneous variations in water status within a vineyard. The information provided by thermal images proved to be relevant at a seasonal scale as well, although it did not match seasonal trends in water status but mimicked other physiological processes occurring during ripening. Therefore, if a picture of variations in water status is required, it would be necessary to acquire thermal images at several dates along the summer.

1. Introduction

In the last two-decades, Precision Agriculture techniques have been progressively implemented in viticulture, giving birth to what is called Precision Viticulture (PV). Along those years, PV has focused on delineating management zones, i.e.: on defining within-vineyard areas that are relatively homogeneous, and different to other areas in the same vineyard (Arno et al., 2011; Arnó et al., 2009; Urretavizcaya et al., 2014). This approach is very appropriate for high-value crops such as grapevine and, when transferred to grape-growing companies, it usually implies adopting site-specific cultural practices for each zone defined (Bramley et al., 2011b; Santesteban et al., 2013; Serrano et al., 2015). In those companies, where new generation grape harvesters are available, the zones delineated can also be used to automatically segregate grapes from the same field into two batches to improve global wine quality (Bramley et al., 2011a; Santos et al., 2012).

* Corresponding author.
E-mail address: gonzaga.santesteban@unavarra.es (L.G. Santesteban).

http://dx.doi.org/10.1016/j.agwat.2016.08.026
0378-3774/

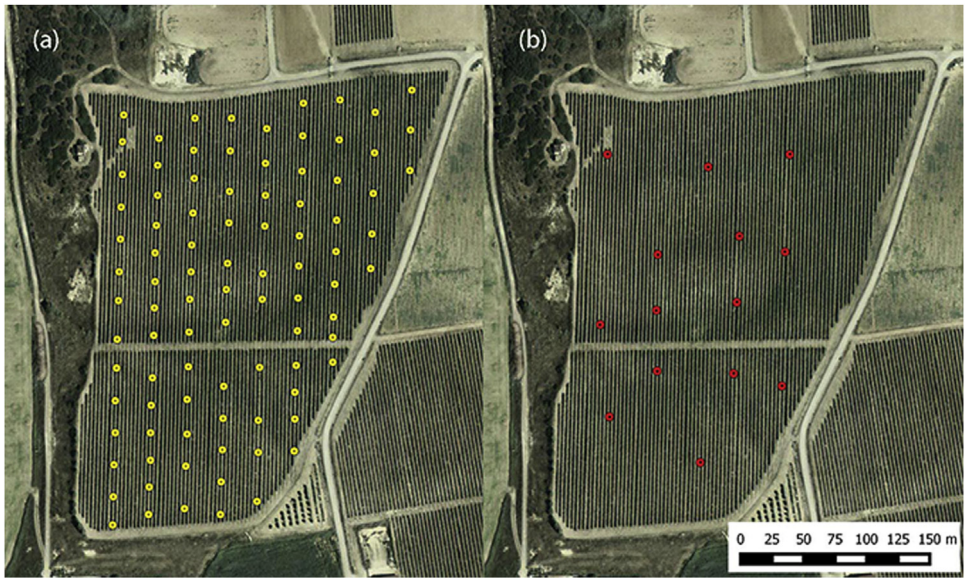

Fig. 1. Aerial view of the vineyard indicating the location of (a) Sampling Points (SP) and (b) Water status Sampling Points (WSP).

The most common sources of information on field spatial variability for zone delineation are (i) vegetation indices obtained from airborne multispectral cameras, (ii) soil apparent conductivity or resistivity, and (iii) data gathered in situ following a sampling grid (Arnó et al., 2009). However, those approaches are not considering any variable directly related to plant water status, which, in semiarid areas, is usually regarded to be the major factor determining grape yield and berry composition (Medrano et al., 2014). Besides, in a context of climate change, water status is also expected to play an increasingly relevant role in cooler areas, as water deficit periods along the growing season are expected to occur more likely in the near future (Ashenfelter and Storchmann, 2016; Fraga et al., 2012; Viguié et al., 2014), so PV approaches should pay much greater attention to water availability.

Whole field imaging using thermal cameras is a source of useful information in this regard, as it allows estimating canopy temperature, known to be related to plant transpiration and, therefore, to plant water status (Jackson et al., 1988, 1981). High resolution thermal cameras have been successfully mounted on aircraft platforms (Sepulcre-Canto et al., 2006) and on unmanned aerial vehicles (UAV), increasingly using higher performance sensors in terms of lower size and weight, and of greater spectral and spatial resolutions. Last generation thermal cameras can reach centimeter ground resolution, providing enough accuracy for canopy extraction in discontinuous crops in rows such as grapevines and fruit trees, and are a promising tool for field and irrigation management applications (Berni et al., 2009; Zarco-Tejada et al., 2012).

In viticulture, proximal thermal sensing has been shown to be a good tool to estimate plant water status (Fuentes et al., 2012; Grant et al., 2007; Jones et al., 2002; Pou et al., 2014). In those approaches, a thermal camera is directly used to get a lateral view, or mounted on a shaft or a crane, to get a zenithal view; and relatively good agreement is observed between canopy-temperature derived indices and plant water potential or stomatal conductance. On the contrary, the implementation of UAV-based thermal imaging solutions has not been well explored yet in viticulture, since the resolution obtained must be sufficient to enable targeting pure canopy pixels, avoiding mixed soil/vegetation pixels (Gonzalez-Dugo et al., 2015), which is particularly complicated in most vineyards due to the structure of the crop, trellised in narrow rows. In one of those works, Baluja et al. (2012a) evaluated the water status variability of a commercial rainfed Tempranillo vineyard using a UAV platform, and observed that some vegetation indices, not derived from thermal images but from multispectral ones, were better correlated to stomatal conductance and leaf water potential, probably as they reflected a longer term response. Another research team also working in Spain, evaluated the correlation between Crop Water Stress Index (CWSI, a canopy-temperature derived index) and leaf water potential, reporting that correlation improved at noon (Bellvert et al., 2014), and exploring the potentiality of the technique for setting thresholds useful for irrigation scheduling (Bellvert et al., 2015a, 2015b).

Gonzalez-Dugo et al. (2013) recently suggested that the requirements to achieve the water stress monitoring using aerial platforms are: (a) establish a strong correlation between stress indices and actual water stress in the field; (ii) the spatial resolution must be sufficient to enable targeting pure canopy pixels, avoiding mixed soil/vegetation pixel; (iii) the ability to evaluate entire fields in individual flight; (iv) faster turn-around acquisition times and processing in order to provide quasi-real time water status maps helping the farmer decision-making process.

The aim of this study is to evaluate the interest of high-resolution UAV-based thermal imaging to estimate the instantaneous and seasonal variability of plant water status within a vineyard. The significance of our approach is that we worked at a commercially realistic scale (7.5 ha), the high resolution of the thermal images acquired (9 cm pixel^{-1}), and that we tested to which extent the information provided by one flight campaign can be used to evaluate spatial variability in water availability across the season.

2. Material and methods

2.1. Vineyard characterization

The experimental work was performed in a 7.5 ha vineyard located in Traibuenas, Navarra, Spain (42°22′20.1″N 1°37′34.2″W, WGS84, Altitude: 328 m), in a region characterized by a semiarid climate (Bs type in Koppen's classification; P < 350 mm; ETP_{Penman} >1150 mm). The vineyard is trained as a vertical shoot positioned bilateral cordon, bud number fixed at 12 buds per m of row line, plant spacing being 3 m between rows and 1 m within the row. The vineyard was 18 years-old at the beginning of the experiment, it was managed according to standard practices in the area, and vines were not affected in a significant way by pests or diseases,

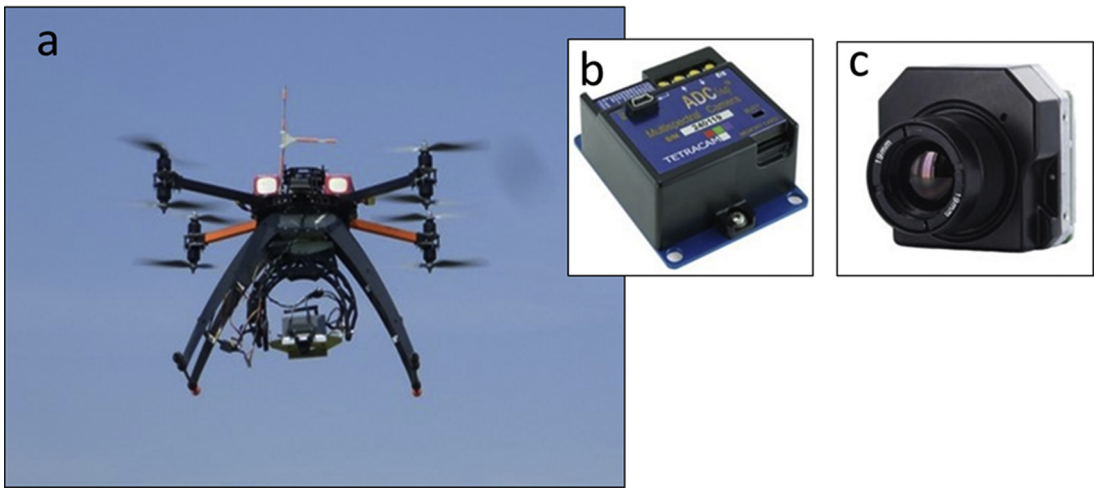

Fig. 2. UAV platform designed for simultaneous data acquisition (a) and detailed view of multispectral (b) and thermal (c) cameras mounted on it.

with the sole exception of approx. 2% of the vines showing slight to moderate esca symptoms.

Spatial variability within the vineyard was characterized setting up two sampling grids. The first one (Fig. 1a), dedicated to the agronomical characterization of the vineyard, was comprised of 92 sampling points (SP), and followed a relatively regular rectangular pattern with a mean distance of 25 × 25 m between SP. The second grid was dedicated to vine water status characterization, followed an irregular pattern (Fig. 1b) conformed by 14 water status measurement points (WSP). On every SP and WSP, 10 vines located at two adjacent rows were marked, and all of them used for the experimental measurements and sampling procedures detailed below.

The agronomical characterization of the 92 SP included the following measurements:

- Vegetative growth, estimated as the total shoot cross sectional area (SCSA) per vine. The basal diameter of all the shoots in the 10 vines in the SP was measured with a hand-held caliper at the end of July, once apical growth had stopped. At winter rest, trunk cross sectional area (TCSA) was determined measuring trunk diameter 30 cm above-ground.
- Yield, determined at harvest by counting and weighting all the clusters produced in the 10 vines at each SP.
- Grape composition at harvest: one 300-berry sample was taken at each SP was taken to determine berry weight (BW) as well as the main composition parameters. After crushing, total soluble solids concentration (TSS) was measured with a temperature compensating refractometer RFM840 (Bellingham-Stanley Ltd., Kent, UK), pH and titratable acidity (TA) using a pH-Burette 24 auto-titrator (Crison, Barcelona, Spain), malic (MalA) and tartaric acid (TarA) concentration was measured enzymatically using an autoanalyzer (Easychem, Systea s.p.a., Italy), whereas yeast assimilable nitrogen (YAN) was estimated following the procedure described by Aerny (1996) with the modifications detailed in Garcia et al. (2011). Total anthocyanins (TAnt) content was evaluated after 4 h extraction at pH = 1.0 following the methodology described in Glories and Augustin (1993).
- Berry carbon isotope ratio ($\delta^{13}C$), measured in 50-berry samples gathered at harvest, then oven-dried and ground into a fine homogeneous powder, and analysed as using an Elemental analyzer (NC2500, Carlo Erba Reagents, Rodano, Italy) coupled to Isotopic Mass Spectrometer (Thermoquest Delta Plus, ThermoFinnigan, Bremen, Germany) as detailed in Santesteban et al. (2012). This measurement was done in 2014 and in 2015.

The characterization of the 14 WSP included, in addition to the agronomic measurements described for the SP, weekly measurements of stem water potential at mid-morning ($\Psi_{s\text{-}m}$) and at noon ($\Psi_{s\text{-}n}$). Measurements were taken from 15 days after fruit set, until harvest time in 2014 and 2015. At each WSP, five healthy leaves were bagged 1.5 h prior to measurement using zip-bags covered with a metalized high-density polyethylene reflective film (SonocoRF, Sonoco Products Co., Hartsville, SC, USA). Stem water potential was determined using a Scholander pressure bomb (P3000, Soil Moisture Corp., Santa Barbara, CA, USA).

Last, we also had information available on soil apparent electric conductivity (ECa) and on Plant Cell Density (PCD) vegetation index. ECa was estimated in December 2014, when soil was at field capacity, at every SP using a handheld EM38 conductivity meter (Geonics Ltd, Ontario, Canada). PCD was calculated as the ratio between RED/NIR bands from images acquired by an airborne RGB-NIR sensor, gathered in a commercial mission performed by a private company (Agropixel SA) on August 10th of 2015. PCD values were normalized to a 8-bit scale (0–255).

2.2. UAV platform and payload

The UAV platform (Fig. 2a) was a modified multi-rotor MikrokopterOktoXL (HiSystems GmbH, Moomerland, Germany), an open-source project described in detail in Matese et al. (2015), which included a pre-assembled hardware and a GPS V3.0 module as positioning system, able to carry a 2 kg payload for 15 min flight time. Flight parameters communication to the ground operator were provided by a radio link at 2.4 GHz, while another channel at 5.8 GHz was used for remote sensing data transmission. The core of the UAV system is a Flight Control board (FlightCtrl), based on an ATMega1284P microcontroller (Atmel Corporation, San Jose, CA, USA), which communicates with the eight brushless controllers by a two-wire bi-directional serial bus (I2C). It integrates a pressure sensor and 3-axis accelerometers to calculate and align the UAV with gravity. The FlightCtrl is linked to a navigation control board (NaviCtrl), equipped with an ARM9 microcontroller (Atmel Corporation, San Jose, CA, USA) and a MicroSD slot card for waypoint data storage. An integrated navigation sensor system based on a 3D digital compass to monitor the z (yaw) axis rotation and a LEA-6 GPS module (U-blox AG, Thalwil, Switzerland) with a circular error of about 2 m, allow various levels of autonomous flight. The UAV mounts eight ATMEGA8 control cards (Atmel Corporation, San Jose, CA, USA), dedicated to the management of each brushless motor with a very quick time response (less than 0.5 ms). The flight plan-

ning was conducted with Mikrokopter Tools software, which allows the user to generate a route of waypoints as a function of the sensor Field Of View (FOV), the degree of overlap between images and the ground resolution needed. A universal camera mount equipped with three servomotors allows a correct image acquisition by correcting the tilt and rolling effects.

A FLIR TAU II 320 (FLIR Systems, Inc., USA) was used for thermal data acquisition. This sensor, optimized for UAV application, is of minimal size (44.5 × 44.5 × 30.0 mm) and weight (72 g). Imaging sensor characteristics, i.e. 324 × 256 pixels and 24° × 18° FOV with fixed focal length of 19 mm, allows obtaining images of about 40 × 30 m at the ground, with a resolution of 0.13 m/pixel at 100 m flight altitude. The camera is equipped with an uncooled sensor able to measure longwave radiation in the spectral range 7.5–13 μm. Radiometric calibration was conducted in the laboratory, using blackbodies under varying target and ambient temperatures to develop radiometric calibration algorithms following the procedure described in Berni et al. (2009).

2.3. Flight campaign

At early veraison (28th July 2015), the site was monitored with a single flight survey at 70 m above ground level at solar noon, providing 9 cm pixel^{-1} ground image resolution. Camera settings were set to a fixed exposure with automatic trigger at 2 s frequency. The waypoint route was generated to obtain 80% overlap both between photos (forward overlap) and between flight lines (lateral overlap), in order to achieve the highest accuracy in mosaicking elaboration step. The images were recorded during homogeneous and stable radiation conditions, under clear sky conditions and with no wind. The thermal acquisition by the UAV was made between 13:00 to 14:30 h by means of five consecutive flights of 15 min each.

Shortly after thermal image acquisition by the UAV (5–10 min later), stem water potential (Ψ_s) and leaf stomatal conductance (g_s) were measured in all the WSP. Ψ_s was measured following the same protocol and sample size used in the weekly measurements of $\Psi_{s\text{-}m}$ and $\Psi_{s\text{-}n}$, wheras g_s was determined in three sunlit leaves per WSP using a hand-held porometer (SC-1, Decagon Devices Inc., Pullman, Washington).

2.4. Image data processing

Leaf emissivity acquired in the thermal infrared spectral region allowed the computation of water stress related to leaf temperature, through the estimation of CWSI (Crop Water Stress Index) using the modified Eq. (1) derived by (Jackson et al., 1988):

$$CWSI = (T_{leaf} - T_{wet})/(T_{dry} - T_{wet}) \quad (1)$$

where T_{dry} and T_{wet} are, respectively, the dry leaf reference temperature representing a stressed leaf temperature and wet leaf temperature reference in total absence of stress, while T_{leaf} indicates the leaf surface temperature. Respect to the original equation defined by Jackson, the modified one uses the canopy temperature (T_{leaf}) instead of the differences between canopy and air temperature (Tc – Ta), moreover identify T_{dry} and T_{wet} as the upper limit $(Tc - Ta)_{UL}$ and the lower limit $(Tc - Ta)_{LL}$ respectively.

T_{leaf} data in absolute temperature (°C) were calculated from thermal camera's digital number (DN) using an empirical line correction. The DN-values in the thermal imagery represent at-sensor radiance. Conversion was carried out in field conditions, by means of three different colour panels (1 × 1 m) at known temperature as reference. Those measurements were achieved at the beginning and the end of each flight and replicated three times with a 10 s delay. The reference target temperature was calculated taking into account the emissivity coefficient of panel material (0.95). The average temperature of the reference targets was 33 °C, 54 °C and 66 °C for the white, blue and black respectively during the entire flight acquisitions. The temperature range of the three panels (black, blue and white) had a variation of 6.6 °C, 3.4 °C and 1.5 °C respectively during the five flights. The averaged values derived from 6 measures for each target and for each flight. The reference temperature (T_{dry} and T_{wet}) estimation procedure is a step that requires utmost care and precision, as it represents a key factor in the stress map computation. CWSI reference measurements were achieved at the end of each flight and replicated three times with a 10 s delay. The emissivity coefficient applied to leaf measurements was 0.98. The average temperature of the T_{dry} reference was 36.1 °C and for Twet 23.6 °C. The temperature range of the T_{dry} and T_{wet} had a variation of about 1.3 °C and 2.4 °C respectively during the five flights. Many studies reported different methods to measure and calculate these references (Alchanatis et al., 2010; Cohen et al., 2005; Grant et al., 2007; Jones et al., 2002; Testi et al., 2008; Yuan et al., 2004). In this work, we preferred the approach suggested by Jones et al. (2002). In detail, leaves of two sampling vines were coated on both sides with petroleum jelly, in order to prevent the leaf transpiration and interrupt the transpiration cooling phenomenon, simulating the leaf physiological response to water stress conditions. At the same time, the wet reference was obtained wetting both sides of other two sampling vines. Temperature monitoring was carried out with a handheld thermal sensor FLIR I7, T_{dry} was measured 30 min after applying petroleum jelly, while T_{wet} 20 s after wetting leaves with water.

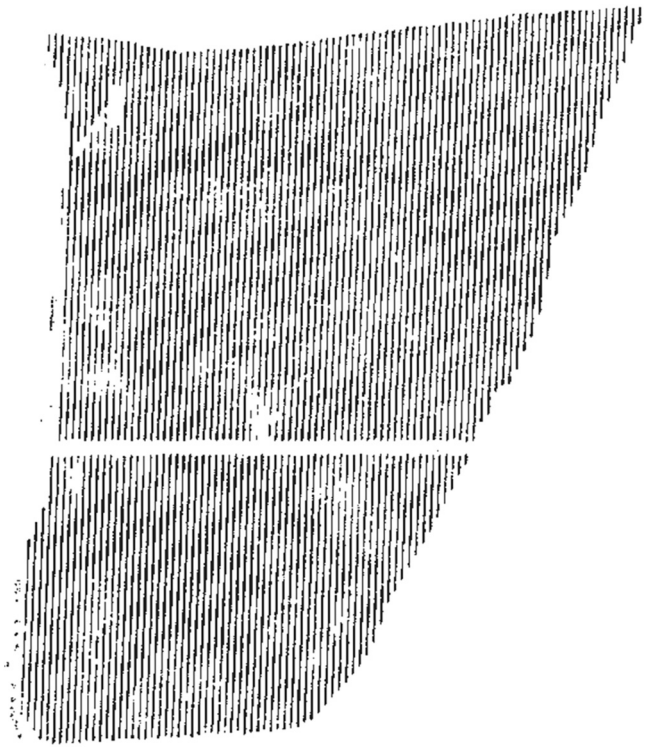

Fig. 3. Filtered map with rows of the vineyard after the soil removing procedure.

Thermal images acquired by UAV were mosaicked using Agisoft Photoscan Professional Edition 1.1.6 (Agisoft LLC, St. Petersburg, Russia), a commercial computer vision software package. This software provides a completely automated computer vision SfM procedure, taking a set of images as input and automatically going through the steps of feature identification, matching and bundle adjustment. The procedure aligns images captured by the thermal camera. A polygon mesh was computed from the dense 3D point, and the pixel values of each image were then projected onto the mesh to create an orthomosaic. When combined with the

Table 1
Descriptive statistics of agronomic characteristics within the vineyard. (a) Data from the sampling point (SP) grid, (b) data from the water status sampling point (WSP) grid. For each variable, mean, minimum (min), maximum (max), standard deviation (sd), coefficient of variation (CV), and percentiles 5, 25, 75 and 95 (p5, p25, p75, p95) are given.

	SP sampling grid								
	mean	min	p5	p25	p75	p95	max	sd	CV
TCSA (cm^2 $vine^{-1}$)	23.2	16.4	18.5	20.9	25.2	29.3	31.3	3.06	13.2
SCSA (mm^2 $vine^{-1}$)	906	558	667	809	995	1173	1224	72.5	8.0
Yield (kg $vine^{-1}$)	3.0	0.7	1.4	2.2	3.8	5.0	5.6	1.09	36.2
BW (g)	1.97	1.52	1.58	1.77	2.14	2.41	2.87	0.25	12.9
TSS (°Baumé)	14.30	12.45	13.14	13.71	14.95	15.45	15.66	0.72	5.0
TA	3.40	2.10	2.80	3.00	3.70	4.30	5.30	0.53	15.7
pH	3.76	3.50	3.60	3.70	3.80	4.00	4.00	0.13	3.3
MalA	2.50	1.50	1.60	2.10	2.80	3.51	4.40	0.55	21.9
TarA	6.8	5.8	6.2	6.4	7.1	7.5	7.8	0.43	6.3
YAN	200	99	131	168	230	284	312	45.7	22.8
TAnt	2248	1624	1767	2000	2497	2724	3158	313	13.9
$\delta^{13}C$ (‰)	−26.4	−27.9	−27.8	−27.2	−25.8	−25.1	−24.1	0.84	3.2
	WSP sampling grid								
	mean	min	p10	p25	p75	p90	max	sd	CV
TCSA (cm^2 $vine^{-1}$)	22.3	17.7	18.2	21.0	23.5	27.2	28.6	2.76	12.4
SCSA (mm^2 $vine^{-1}$)	902	667	713	831	971	1116	1181	128.7	14.3
Yield (kg $vine^{-1}$)	3.5	1.4	1.7	2.6	4.2	5.2	5.3	1.12	32.1
BW (g)	2.02	1.82	1.83	1.89	2.19	2.21	2.22	0.15	7.5
TSS (°Baumé)	14.23	13.05	13.13	13.92	14.65	15.09	15.13	0.61	4.3
TA	3.30	2.74	2.83	3.17	3.50	3.53	3.54	0.24	7.3
pH	3.79	3.63	3.65	3.70	3.89	3.92	3.93	0.09	2.4
MalA	2.59	1.80	1.95	2.30	2.90	2.95	3.00	0.35	13.4
TarA	6.6	6.2	6.3	6.5	6.9	7.0	7.0	0.23	3.5
YAN	202	150	163	187	219	241	249	25.5	12.6
TAnt	2248	1915	1946	2127	2422	2518	2529	191	8.5
$\delta^{13}C$ (‰)	−25.7	−27.5	−26.9	−26.1	−25.1	−24.6	−24.4	0.76	3.0

TCSA: trunk cross-sectional area; SCSA: sum of shoot cross sectional area; BW: berry weight; TSS: total soluble solids; TA: titratable acidity; MalA: malic acid; TarA: tartaric acid; YAN: Yeast available nitrogen; TAnt: total anthocyanins; $\delta^{13}C$: carbon isotope ratio. SP: sampling-point; WSP: water-status sampling point.

GPS positions, this process allows the creation of a high-resolution orthophoto and a digital elevation model (DEM) of the research site.

2.5. Row extraction and spatial analysis

The DEM output from Agisoft software allowed developing a filtering procedure of the pure row pixels, since they have greater heights from the ground, and can be easily discriminated by global thresholding algorithms. The first step was to applicate the Top-Hat morphological operation (Gonzalez and Wintz, 2002) directly on the DEM image. Through this technique, usually used for non-uniform illumination correction, we made "flat" the terrain that may in fact be pending. Then, using a global thresholding method (Otsu et al., 1979), two different zones were obtained: rows and ground. The Otsu method discriminates the two classes automatically determining a threshold that maximizes the interclass variance. The purpose of this procedure is to split the image f (x, y) in two parts (row and inter-row), imposing a threshold on the histogram image intensity that, in this case, coincides with the height. DEM rows in the image have a height, then intensity, almost constant, consistent with each other and always more than the ground. Data extraction for single plants was made averaging values in 0.8 × 0.3 m polygons along rows (Fig. 3), polygon size being chosen to properly identify each plant from the adjacent ones.

2.6. Evaluation of the relationship between CWSI and plant water status

In order to evaluate the instantaneous correspondence between water status characterization through standard proxy techniques and thermal imagery, the Ψ_s and g_s values measured at the WSP in the flight campaign day were compared to their CWSI through regression analysis.

At the seasonal scale, the evaluation of the appropriateness of thermal images acquired at one date to estimate seasonal variability in water status along the field was done through a spatial modeling approach. Spatial modeling of leaf water potential along the vineyard was done according to the approach proposed by Acevedo-Opazo et al. (2010a, 2010b, 2008). In this approach, one (or more) ancillary variable(s), whose spatial distribution is well known, is combined with plant water status information at a reference site to elaborate a model that estimates plant water status.

In our paper, we used the same procedure considered by Herrero-Langreo et al. (2013), where more details on the methodology can be found. Following that procedure, we considered carbon isotope ratio ($\delta^{13}C$) measured at the 92 SP in the previous season as the ancillary variable, and the most stressed WSP as the reference site. The model was calibrated and tested using the measurements of Ψ_s at all the WSP, considering the measurements made weekly in 2014 and 2015. Seasonal average leaf water potential at each SP could then be estimated from the model. Independent models were calculated for $\Psi_{s\text{-}m}$ and $\Psi_{s\text{-}n}$. Following the empirical approach proposed by Acevedo-Opazo et al. (2008), the spatial model tested in this study, is shown in Eq. (2).

$$\hat{\Psi}\left(s_i, t_j\right) = \left(b_0 + b_1.\delta^{13}C\left(s_i\right)\right).\Psi\left(s_{re}, t_j\right) \quad (2)$$

Where

s_i corresponds to any of the 92 locations where a $\delta^{13}C$ value was measured

s_{re} corresponds to the reference site, where Ψ was measured throughout 18 dates.

t_j corresponds to any of the 18 dates when Ψ was measured at the reference site, s_{re}

$\hat{\Psi}\left(s_i, t_j\right)$ is the estimated Ψ at each site, s_i, and date, t_j.

$\delta^{13}C\left(s_i\right)$ is the auxiliary variable, $\delta^{13}C$, at each site, s_i.

$\Psi\left(s_{re}, t_j\right)$ is Ψ measured at the reference site, s_{re}, for each date t_j.

b_0 and b_1 are the coefficients of the model

For each date, t_j, the model extrapolates Ψ measured at the reference site, $\Psi(S_{re}, t_j)$, to any of the locations, si, where a $\delta^{13}C$ value was measured. Hence, $\delta^{13}C$ (s), accounts for the spatial variability of Ψ, while temporal variation is indicated by $\Psi\left(s_{re}, t_j\right)$. The model was adapted to the case study following the same procedure considered by Herrero-Langreo et al. (2013) where a more extensive explanation on the methodology can be found.

The comparison between CWSI and average seasonal $\Psi_{s\text{-}m}$ and $\Psi_{s\text{-}n}$ values was done using two different procedures. First, we interpolated maps for those variables onto a 3×3 m grid using block kriging performed with VESPER software (Minasny and McBratney, 2002), and compared them visually. Kriging is an interpolation procedure in which estimates of values at unsampled sites are interpolated on the basis of known values at georeferenced locations, weighted according to the parameters of the variogram – a model that describes variation within a dataset as a function of the distance or lag separating the samples comprising it (Bramley et al., 2011b). In our work, all variables were fitted to exponential models, taking as kriging parameters maximum distance = 100 m, 30 lags and 50% of lag tolerance. The second procedure for comparison was classifying CWSI in 3 and 5 classes through *fuzzy k-means* cluster analysis, and then calculating mean $\Psi_{s\text{-}m}$ and $\Psi_{s\text{-}n}$ values for pixels belonging to each class with $P > 0.8$. *Fuzzy k-means* analyses and boxplots were obtained using R software.

3. Results and discussion

3.1. Within-vineyard variability of agronomic variables

The vineyard considered showed a relatively wide range of within-vineyard variability concerning vegetative growth, yield, berry weight and grape composition (Table 1a). In general terms, the range of variability embraced was high for all variables and the coefficients of variation were twice those reported in previous studies for the same variety in a neighbouring region (Baluja et al., 2012b; Urretavizcaya et al., 2016). That variability makes the field suitable for a precision viticulture based management (Urretavizcaya et al., 2014), aimed at decreasing variability or at segregating grape batches according to their composition. Although within-vineyard average values can be considered as adequate for quality wine making – according to regional standards for the variety-, the presence of less-ripen or "greener" grapes would impact negatively in wine organoleptic quality (Kontoudakis et al., 2011).

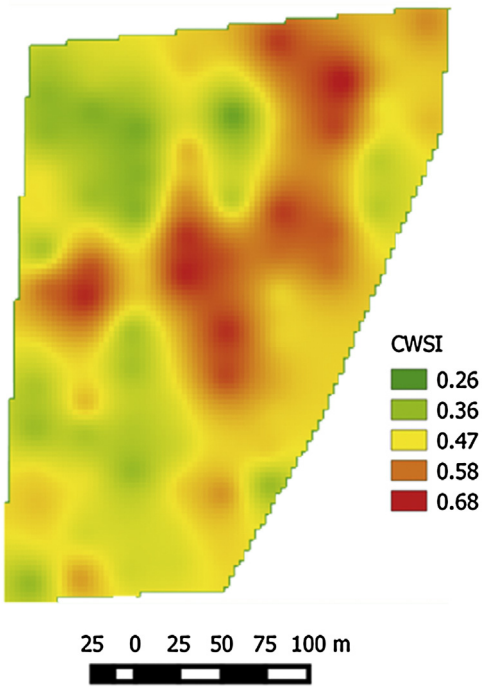

Fig. 4. Variation in Crop Water Stress Index (CWSI) in the 7.5 ha cv- 'Tempranillo' vineyard.

Within-field variability in vine water status was also remarkable, $\delta^{13}C$ ranging from −24.1‰ to −27.9‰ (Table 1a). These values, according to the scale proposed in (Santesteban et al., 2015), correspond to conditions ranging from nearly severe water stress to weak deficit. This variability in water status probably explains the variability in other agronomical variables, since water availability is known to be the major factor determining growth, yield and grape composition in semiarid areas (Medrano et al., 2014).

The range of variability embraced by the WSP grid was smaller (Table 1b), but represented well the range of conditions observed in the denser SP grid. In fact, in most cases, WSP maximum and minimum values were similar to percentiles 5–95 in the SP grid, indicating that, in general terms, 90% of within-vineyard variability is covered by the WSP grid.

3.2. Evaluation of the instantaneous variability in water status through thermal images

Thermal image processing led to a map of CWSI distribution along the field (Fig. 4). A wide range of CWSI values was found (0.28–0.69), confirming the relevance of within-field variability observed with agronomic variables, and the pertinence of taking into account this variability. When CWSI values obtained from thermal images for the WSP were compared to instantaneous measurements in the field, they showed a relatively good correspondence with both Ψs and g_s (Fig. 5, $R^2 > 0.65$, $P < 0.01$), presenting lower values of Ψ_s and g_s at the WSP with higher CWSI. The coefficients of determination are relatively high partly as one of the points monitored was clearly more stressed than the remaining ones, so when little variation in within-field water status exists correlation can be expected to be lower.

The results obtained agree with those observed for thermal imaging in vineyards, either using a proxy (Fuentes et al., 2012; Grant et al., 2007; Jones et al., 2002; Pou et al., 2014) or a remote (Baluja et al., 2012a; Bellvert et al., 2015a,b, 2014) sensing approach. According to the principles established in early research regarding temperature sensing as an estimator of plant water status, plants having a greater water availability usually show increased transpiration, which leads to certain evaporative cooling and, as a consequence, to lower leaf temperature (Jackson et al., 1988, 1981). Therefore, from this point of view, our results add further evidence on the suitability of this approach, and reinforce the potential role UAV thermal imaging may have as an instantaneous water-stress mapping tool.

3.3. Evaluation of the seasonal variability in water status through thermal images

Spatial modeling of stem water potential applied following the approach proposed by Acevedo-Opazo et al. (2010a, 2010b, 2008) proved to be successful. The model allowed a good estimation of $\Psi_{s\text{-}m}$ and $\Psi_{s\text{-}n}$ at the WSP using the most stressed WSP as the reference site, and carbon isotope ratio measured the previous season ($\delta^{13}C$) in the SP as ancillary information (Fig. 6). Thus, it could then be used to estimate $\Psi_{s\text{-}m}$ and $\Psi_{s\text{-}n}$ values at the SP, subsequently

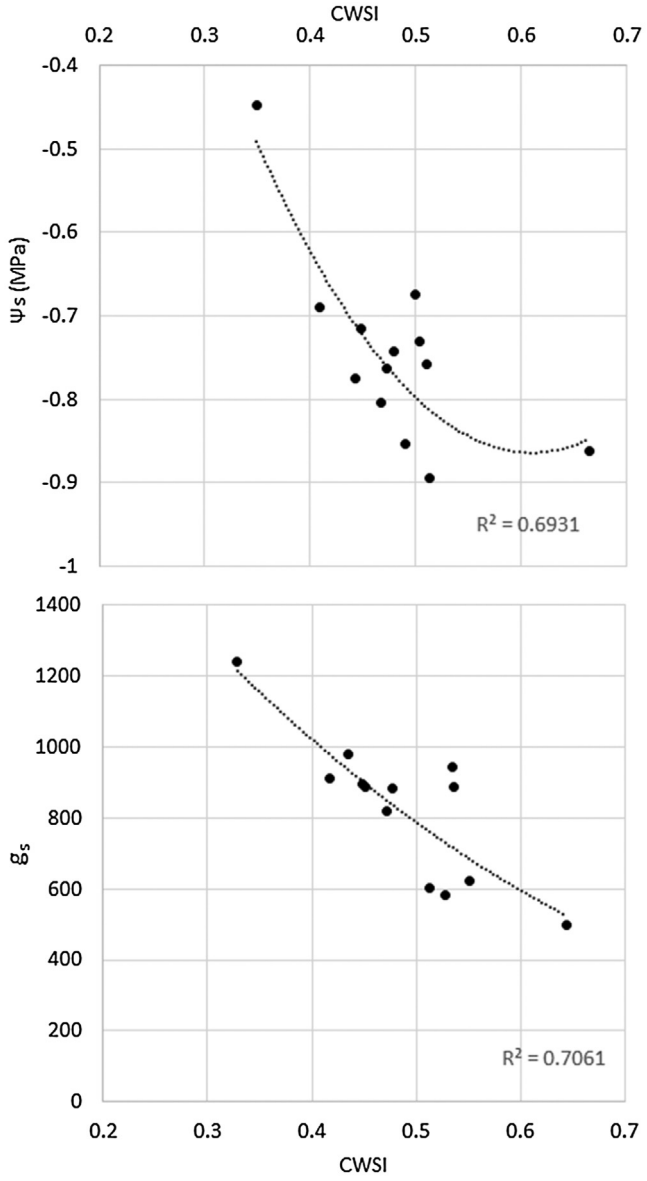

Fig. 5. Comparison of Crop Water Stress Index values calculated from UAV-acquired thermal images and (a) stem water potential and (b) stomatal conductance measured at the WSP at the same time.

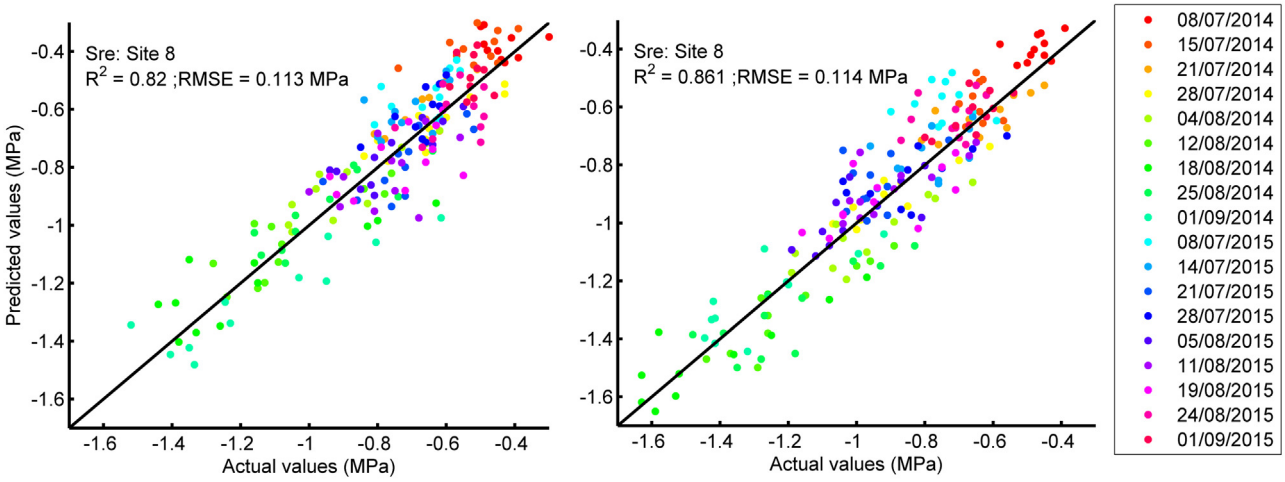

Fig. 6. Plot of observed vs estimated values for (a) stem water potential at mid-morning ($\Psi_{s\text{-}m}$) and (b) noon ($\Psi_{s\text{-}n}$) stem water potential. Estimation was performed using as ancillary information $\delta^{13}C$ measured in the previous season. Water potential measurement dates are identified in colours (1–9: 2014; 10–18: 2015).

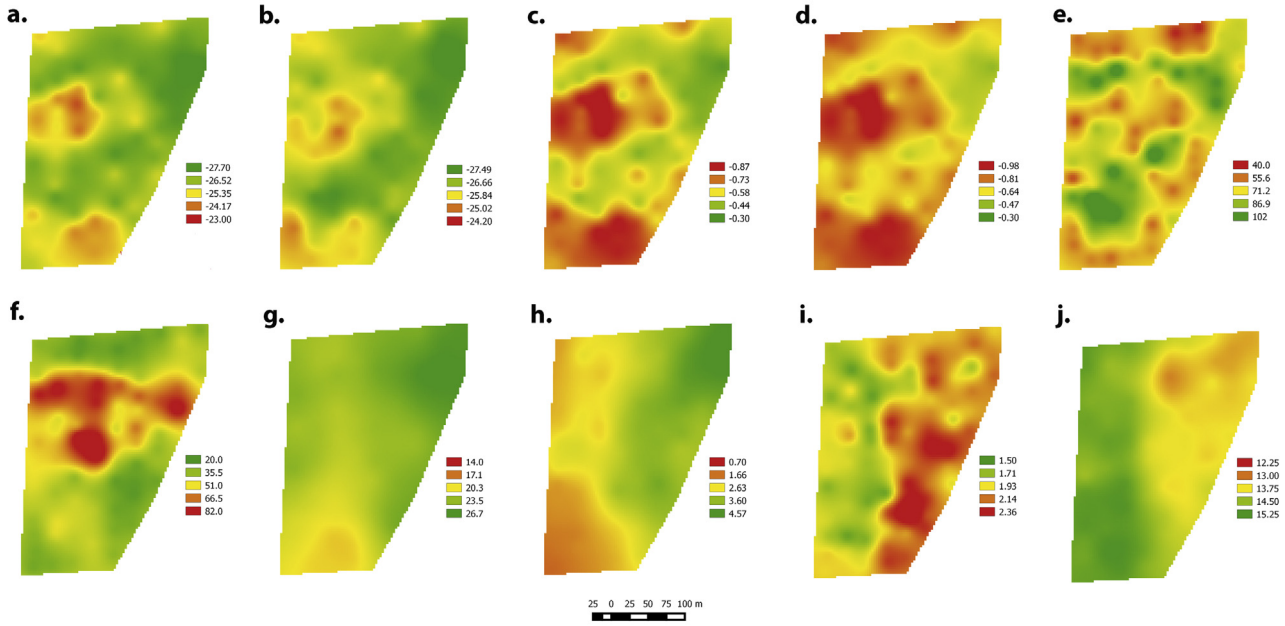

Fig. 7. Maps of variations along the vineyard of: (a) carbon isotope ratio – 2014 ($\delta^{13}C_{2014}$, ‰); (b) carbon isotope ratio – 2015 ($\delta^{13}C_{2014}$, ‰); (c) mid-morning ($\Psi_{s\text{-}m}$) and (d) noon ($\Psi_{s\text{-}n}$) stem water potential (MPa); (e) Plant Cell Density (PDC, expressed in a 0-255 8-bit scale); (f) soil apparent electrical conductivity (ECa, mS cm^{-1}); (g) trunk cross-sectional area (TCSA, cm^2 vine^{-1}); (h) yield (kg vine^{-1}); (i) berry weight (BW, g); (j) total soluble solids (TSS, ◦Baume).

represented as maps in Fig. 7(c, d), which displays how water status varied within the field.

a. Visual comparison of spatial patterns

From the visual comparison of the maps showed in Fig. 7, a recurrent spatial pattern, roughly agreeing to the topography of the field, can be observed for PCD, $\delta^{13}C_{2014}$ and $\delta^{13}C_{2015}$ datasets, which had been obtained independently. This pattern had also clear resemblances to ECa map, where a horizontal strip of higher ECa values matched areas of higher PCD and $\delta^{13}C$ values. This coherence was not detected for the bottom-left part of the map, where ECa showed intermediate or even low values, whereas relatively high values of PCD, $\delta^{13}C_{2014}$ and $\delta^{13}C_{2015}$ were observed. ECa measurements are probably integrating several soil characteristics of different relevance for plant performance, which explain those differences in behaviour (Brevik et al., 2006). The spatial distribution of $\Psi_{s\text{-}m}$ and $\Psi_{s\text{-}n}$ also followed the general pattern described above, although differences were attenuated at the right-top of the map, and exacerbated at the right-bottom. Last, the distribution pattern of classic agronomic variables followed a very different structure, the eastern (right) part of the field showing higher values of plant trunk section (TCSA), yield and berry weight (BW), and lower berry sugar content (TSS). CWSI estimated from thermal imaging followed a pattern that could be interpreted as a combination of the two major patterns described above (Fig. 4). On one side, a horizontal strip of higher CWSI appeared in the middle of the field, though much milder levels of water stress were detected at the lower part of the map. On the other side, certain degree of differentiation between the left and the right part of the map can also be appreciated.

It is interesting to highlight that the highest CWSI values were found at the right-top of the map, corresponding exactly with the biggest and most productive vines. This behaviour, can be regarded as anomalous at first sight, but matches the water dynamics in this vineyard. According to the expert knowledge of the technical staff in the owning winery, that area has a deep soil, but much more gravely than the rest of the field and, as a consequence, lower water holding capacity. According to owners experience, that part of the field usually shows a very active growth in spring and early summer, and usually a high crop. However, when deficit conditions occur – from July on – soil water depletion happens faster, and plants end the season with greater water stress than other parts in the field. This behaviour can be explained as higher leaf area (Reynolds and Heuvel, 2009) and higher crop load (Miller et al., 1997; Naschitz and Naor, 2005) enhance water consumption and, as a consequence, can result in decreased water reservoirs from mid-season on.

Thus, although at some fields information provided by CWSI could be redundant to that provided by vegetation indices, such as NDVI or PCD, it was not the case in this vineyard. It is common to assume that higher vigour areas will experience milder water stress, but under some circumstances such as those described here (deeper soils with lower water holding capacity), some parts of the field having greater leaf area (estimated through PCD), could experience higher water deficit at the end of the season.

b. Correspondence between CWSI classes and other variables

CWSI pixel values were classified in three and five classes using *fuzzy k-means*. For each class, the values of the remaining variables calculated for each pixel were examined through boxplots (Figs. 8 and 9). When three classes were defined (Fig. 8), the correspondence between CWSI classes and seasonal water status related parameters was very low. Only a certain trend to lower $\delta^{13}C_{2015}$ for increasing values of CWSI was observed, and no correspondence at all for $\Psi_{s\text{-}m}$ and $\Psi_{s\text{-}n}$. However, there was a much higher degree of agreement between CWSI and other variables. PCD was observed to be higher at lower CWSI and, specially, very neat correspondence was found between CWSI and agronomical variables, higher CWSI plants showing higher values of TCSA, higher yields, bigger berries and a decreased sugar content (TSS). When cluster analysis was used to define five CWSI classes (Fig. 9), a very similar pattern was found, CWSI holding a clearer relationship with yield, berry weight and sugar content than water status related variables.

Therefore, CWSI measured at early veraison estimated very well what was happening from an agronomic point of view between the onset of ripening (occurring at the time of measurement)

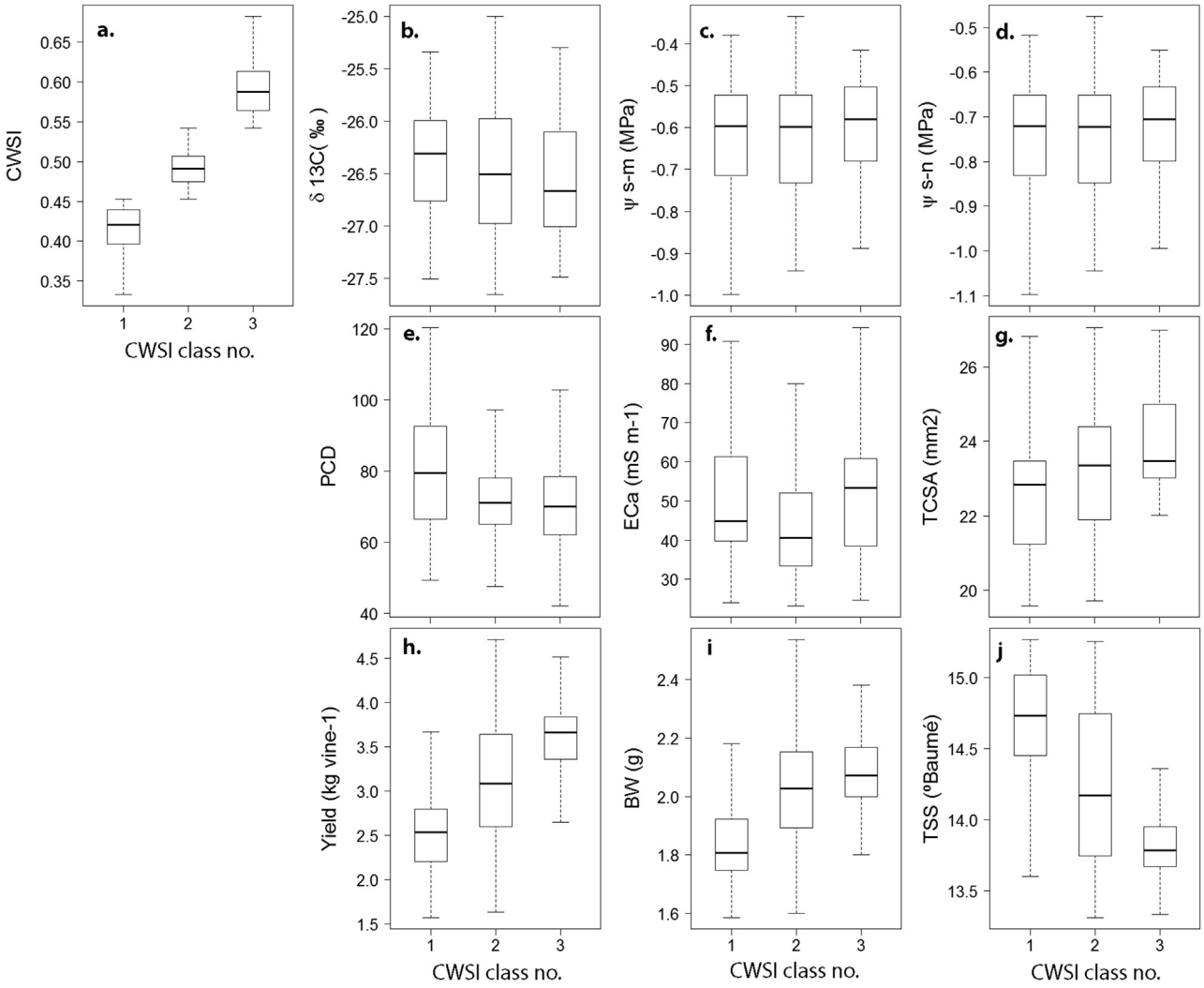

Fig. 8. Correspondence of the 3 classes defined using Crop Water Stress Index (CWSI) and (a) CWSI; (b) carbon isotope ratio – 2015 ($\delta^{13}C_{2014}$, ‰); (c) mid-morning ($\Psi_{s\text{-}m}$) and (d) noon ($\Psi_{s\text{-}n}$) stem water potential (MPa); (e) Plant Cell Density (PDC); (f) soil apparent electrical conductivity (ECa, mS cm^{-1}); (g) trunk cross-sectional area (TCSA, cm^2 $vine^{-1}$); (h) yield (kg $vine^{-1}$); (i) berry weight (BW, g); (j) total soluble solids (TSS, °Baume).

and harvest. High CWSI classes were precisely those that had greater yield and bigger berries (Fig. 8h, i; Fig. 9h, i), and showed a delayed sugar accumulation (lower TSS, Figs. 8j and 9j). Variations in crop (sink size) have already been shown to play a major role to explain within-vineyard variations in grape composition in semi-arid areas (Urretavizcaya et al., 2016), as it constitutes one of the two components of source-to-sink balance, critical for grape quality (Howell, 2001). As mentioned above, higher yields enhance water consumption (Miller et al., 1997; Naschitz and Naor, 2005), and also cause lower sugar contents (Edson et al., 1995; Naor et al., 1997), especially under deficit conditions (Santesteban et al., 2011).

On the contrary, CWSI measured at a single day did not provide a good estimation of variations of plant water status. The vineyard considered in the study showed a stable structure of variation in seasonal water status, as there was a big resemblance between berry $\delta^{13}C$ measured in 2014 and 2015 (Fig. 7a, b). This stability agrees with that observed for water status in other vineyards when several years were compared (Acevedo-Opazo et al., 2010b; Herrero-Langreo et al., 2013; Taylor et al., 2010). The relationship between berry $\delta^{13}C$ and water status has been widely proved for cv. 'Tempranillo' (Santesteban et al., 2012), and it is sensible to consider this spatial structure mirrors stem water potential pattern, estimated here through modeling. The fact CWSI measured in a single – but representative – day did not follow this seasonal pattern cannot be regarded to be indicative of a bad performance for this index (or for this data acquisition platform). In fact, high CWSI pixels corresponded to high yielding parts of the field where sugar accumulation was observed to be limited, possibly as during the last weeks before harvest available water was not enough for such a leaf area and crop load. Thus, CWSI calculated from high-resolution UAV-based thermal imaging has shown a high potentiality for precision vineyard management applications, and could be a complementary tool for the implementation of precision irrigation systems that, in the near future, would help grape growers to manage water resources in a sounder and more sustainable way.

4. Conclusions

UAV-based thermal imagery has a great potential to map instantaneous variations in water status within a vineyard. The information provided by thermal images proved to be relevant at a seasonal scale as well, although it did not match seasonal trends in water status, but mimicked other physiological processes occurring during ripening. Therefore, if a picture of variations in water

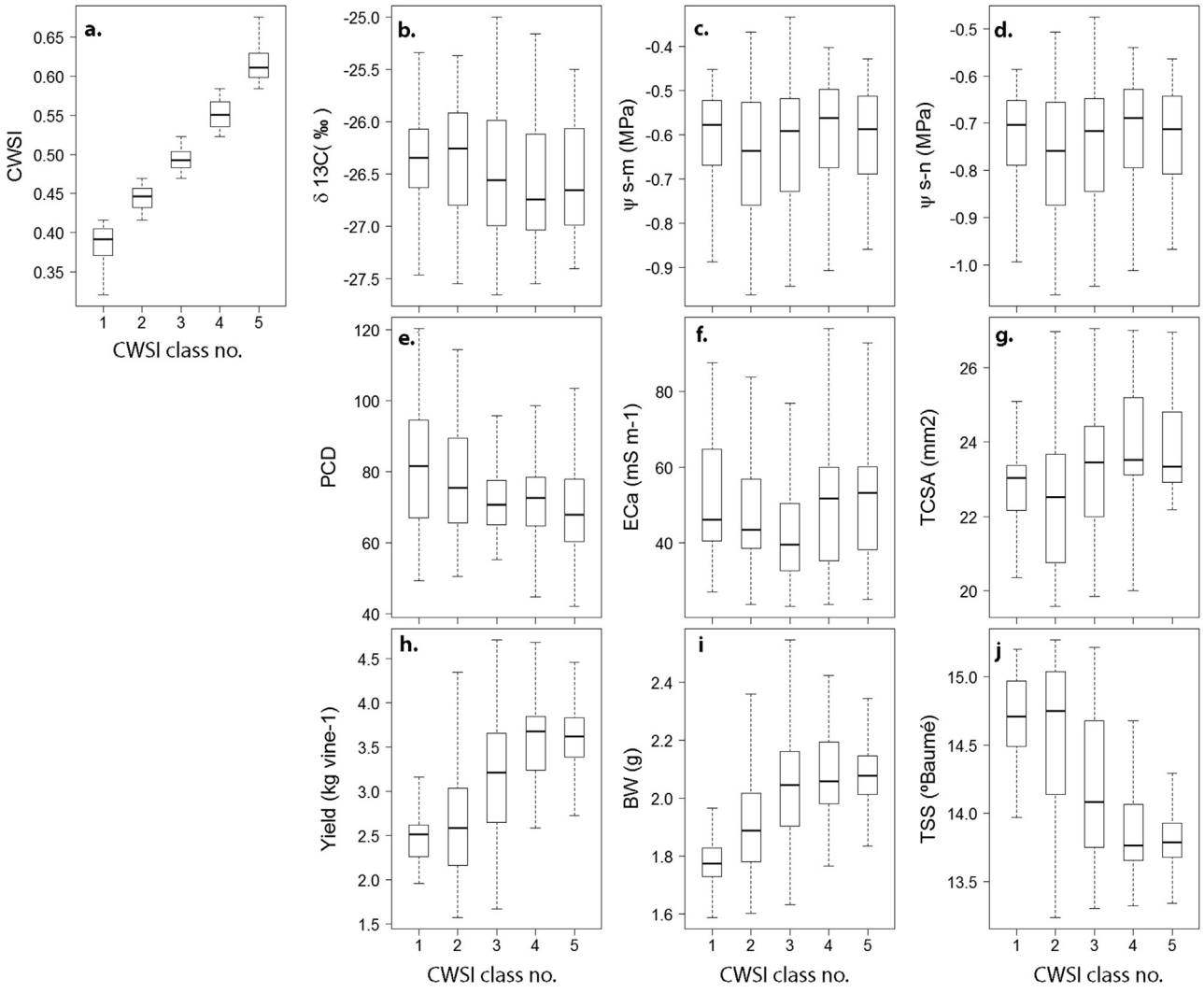

Fig. 9. Correspondence of the 5 classes defined using Crop Water Stress Index (CWSI) and (a) CWSI; (b) carbon isotope ratio – 2015 ($\delta^{13}C_{2014}$, ‰); (c) mid-morning ($\Psi_{s\text{-}m}$) and (d) noon ($\Psi_{s\text{-}n}$) stem water potential (MPa); (e) Plant Cell Density (PDC); (f) soil apparent electrical conductivity (ECa, mS cm^{-1}); (g) trunk cross-sectional area (TCSA, cm^2 vine^{-1}); (h) yield (kg vine^{-1}); (i) berry weight (BW, g); (j) total soluble solids (TSS, ◦Baume).

status is required, it would be necessary to acquire thermal images at several dates along the summer.

Conflict of interest

None.

Acknowledgements

This research was supported by the Industry Dpt of the Government of Navarre (VITICS, Ref: IIM14244.RI1, co-funded by the EU as part of the ERDF program), and by the Italian MIUR (Progetto Premiale AQUA to CNR). The authors also want to thank Bodegas Ochoa, owners of the vineyard where all experiments were made, for their kindness and interest.

References

Acevedo-Opazo, C., Tisseyre, B., Guillaume, S., Ojeda, H., 2008. The potential of high spatial resolution information to define within-vineyard zones related to vine water status. Precis. Agric. 9, 285–302.

Acevedo-Opazo, C., Tisseyre, B., Ojeda, H., Guillaume, S., 2010a. Spatial extrapolation of the vine (Vitis vinifera L.) water status: a first step towards a spatial prediction model. Irrig. Sci. 28, 143–155, http://dx.doi.org/10.1007/s00271-009-0170-3.

Acevedo-Opazo, C., Tisseyre, B., Taylor, J.A., Ojeda, H., Guillaume, S., 2010b. A model for the spatial prediction of water status in vines (Vitis vinifera L.) using high resolution ancillary information. Precis. Agric. 11, 358–378, http://dx.doi.org/10.1007/s11119-010-9164-7.

Aerny, J., 1996. Composés azotés des moûts et des vins. Rev. Suisse Vitic. Arboric. Hortic. 28, 161–165.

Alchanatis, V., Cohen, Y., Cohen, S., Moller, M., Sprinstin, M., Meron, M., Tsipris, J., Saranga, Y., Sela, E., 2010. Evaluation of different approaches for estimating and mapping crop water status in cotton with thermal imaging. Precis. Agric. 11, 27–41, http://dx.doi.org/10.1007/s11119-009-9111-7.

Arnó, J., Martinez-Casasnovas, J.A., Ribes-Dasi, M., Rosell, J.R., 2009. Review. Precision Viticulture. Research topics, challenges and opportunities in site-specific vineyard management. Span. J Agric. Res. 7, 779–790.

Arno, J., Martinez-Casasnovas, J.A., Ribes-Dasi, M., Rosell, J.R., 2011. Clustering of grape yield maps to delineate site-specific management zones. Span. J. Agric. Res. 9, 721–729.

Ashenfelter, O., Storchmann, K., 2016. The economics of wine, weather, and climate change. Rev. Environ. Econ. Policy 10, 25–46, http://dx.doi.org/10.1093/reep/rev018.

Baluja, J., Diago, M.P., Balda, P., Zorer, R., Meggio, F., Morales, F., Tardaguila, J., 2012a. Assessment of vineyard water status variability by thermal and multispectral imagery using an unmanned aerial vehicle (UAV). Irrig. Sci. 30, 511–522, http://dx.doi.org/10.1007/s00271-012-0382-9.

Baluja, J., Tardaguila, J., Ayestaran, B., Diago, M.P., 2012b. Spatial variability of grape composition in a Tempranillo (Vitis vinifera L.) vineyard over a 3-year survey. Precis. Agric., 1–19.

Bellvert, J., Zarco-Tejada, P.J., Girona, J., Fereres, E., 2014. Mapping crop water stress index in a Pinot-noir vineyard: comparing ground measurements with thermal remote sensing imagery from an unmanned aerial vehicle. Precis. Agric. 15, 361–376, http://dx.doi.org/10.1007/s11119-013-9334-5.

Bellvert, J., Marsal, J., Girona, J., Zarco-Tejada, P.J., 2015a. Seasonal evolution of crop water stress index in grapevine varieties determined with high-resolution remote sensing thermal imagery. Irrig. Sci. 33, 81–93, http://dx.doi.org/10.1007/s00271-014-0456-y.
Bellvert, J., Zarco-Tejada, P.J., Marsal, J., Girona, J., González-Dugo, V., Fereres, E., 2015b. Vineyard irrigation scheduling based on airborne thermal imagery and water potential thresholds. Aust. J. Grape Wine Res., http://dx.doi.org/10.1111/ajgw.12173.
Berni, J., Zarco-Tejada, P.J., Suarez, L., Fereres, E., 2009. Thermal and narrowband multispectral remote sensing for vegetation monitoring from an unmanned aerial vehicle. IEEE Trans. Geosci. Remote Sens. 47, 722–738, http://dx.doi.org/10.1109/tgrs.2008.2010457.
Bramley, R.G.V., Ouzman, J., Thornton, C., 2011a. Selective harvesting is a feasible and profitable strategy even when grape and wine production is geared towards large fermentation volumes. Aust. J. Grape Wine Res. 17, 298–305, http://dx.doi.org/10.1111/j.1755-0238.2011.00151.x.
Bramley, R.G.V., Trought, M.C.T., Praat, J.P., 2011b. Vineyard variability in Marlborough, New Zealand: characterising variation in vineyard performance and options for the implementation of Precision Viticulture. Aust. J. Grape Wine Res. 17, 83–89, http://dx.doi.org/10.1111/j.1755-0238.2010.00119.x.
Brevik, E.C., Fenton, T.E., Lazari, A., 2006. Soil electrical conductivity as a function of soil water content and implications for soil mapping. Precis. Agric., http://dx.doi.org/10.1007/s11119-006-9021-x.
Cohen, Y., Alchanatis, V., Meron, M., Saranga, Y., Tsipris, J., 2005. Estimation of leaf water potential by thermal imagery and spatial analysis. J. Exp. Bot. 56, 1843–1852.
Edson, C.E., Howell, G.S., Flore, J.A., 1995. Influence of crop load on photosynthesis and dry matter partitioning of Seyval grapevines. II. Seasonal changes in single leaf and whole vine photosynthesis. Am. J. Enol. Vitic. 46, 469–477.
Fraga, H., Malheiro, A.C., Moutinho-Pereira, J., Santos, J.A., 2012. An overview of climate change impacts on European viticulture. Food Energy Secur. 1, 94–110, http://dx.doi.org/10.1002/fes3.14.
Fuentes, S., de Bei, R., Pech, J., Tyerman, S., 2012. Computational water stress indices obtained from thermal image analysis of grapevine canopies. Irrig. Sci. 30, 523–536, http://dx.doi.org/10.1007/s00271-012-0375-8.
Garcia, S., Santesteban, L.G., Miranda, C., Royo, J.B., Garcia, S., Miranda, C., Royo, J.B., García, S., Santesteban, L.G., Miranda, C., Royo, J.B., 2011. Variety and storage time affect the compositional changes that occur in grape samples after frozen storage. Aust. J. Grape Wine Res. 17, 162–168, http://dx.doi.org/10.1111/j.1755-0238.2011.00134.x.
Glories, Y., Augustin, M., 1993. Maturité phénolique du raisin, conséquences technologiques: application aux millésimes 1991 et 1992. In: Journée Technique Du C.I.V.B. Actes Du Colloque, Bordeaux.
Gonzalez, R.C., Wintz, P., 2002. In: Leonardo (Ed.), Digital Image Processing. , 2nd edition. Prentice Hall, New Jersey, http://dx.doi.org/10.2307/1574313.
Gonzalez-Dugo, V., Zarco-Tejada, P., Nicolás, E., Nortes, P.A., Alarcón, J.J., Intrigliolo, D.S., Fereres, E., 2013. Using high resolution UAV thermal imagery to assess the variability in the water status of five fruit tree species within a commercial orchard. Precis. Agric. 14, 660–678, http://dx.doi.org/10.1007/s11119-013-9322-9.
Gonzalez-Dugo, V., Goldhamer, D., Zarco-Tejada, P.J., Fereres, E., 2015. Improving the precision of irrigation in a pistachio farm using an unmanned airborne thermal system. Irrig. Sci. 33, 43–52, http://dx.doi.org/10.1007/s00271-014-0447-z.
Grant, O.M., Tronina, L., Jones, H.G., Chaves, M.M., 2007. Exploring thermal imaging variables for the detection of stress responses in grapevine under different irrigation regimes. J. Exp. Bot. 58, 815–825.
Herrero-Langreo, A., Tisseyre, B., Goutouly, J.P., Scholasch, T., van Leeuwen, C., 2013. Mapping grapevine (Vitis vinifera L.) water status during the season using carbon isotope ratio (Îí13C) as ancillary data. Am. J. Enol. Vitic. 64, 307–315.
Howell, G.S., 2001. Sustainable grape productivity and the growth-yield relationship: a review. Am. J. Enol. Vitic. 52, 165–174.
Jackson, R.D., Idso, S.B., Reginato, R.J., Pinter, P.J., 1981. Canopy temperature as a crop water stress indicator. Water Resour. Res. 17, 1133–1138.
Jackson, R.D., Kustas, W.P., Choudhury, B.J., 1988. A reexamination of the crop water stress index. Irrig. Sci. 307, 309.
Jones, H.G., Stoll, M., Santos, T., de Sousa, C., Chaves, M.M., Grant, O.M., 2002. Use of infrared thermography for monitoring stomatal closure in the field: application to grapevine. J. Exp. Bot. 53, 2249–2260.
Kontoudakis, N., Esteruelas, M., Fort, F., Canals, J.M., De Freitas, V., Zamora, F., 2011. Influence of the heterogeneity of grape phenolic maturity on wine composition and quality. Food Chem. 124, 767–774, http://dx.doi.org/10.1016/j.foodchem.2010.06.093.
Matese, A., Toscano, P., Di Gennaro, S.F., Genesio, L., Vaccari, F.P., Primicerio, J., Belli, C., Zaldei, A., Bianconi, R., Gioli, B., 2015. Intercomparison of UAV, aircraft and satellite remote sensing platforms for precision viticulture. Remote Sens. 7, 2971–2990, http://dx.doi.org/10.3390/rs70302971.
Medrano, H., Tomás, M., Martorell, S., Escalona, J.-M., Pou, A., Fuentes, S., Flexas, J., Bota, J., 2014. Improving water use efficiency of vineyards in semi-arid regions. A review. Agron. Sustain. Dev., http://dx.doi.org/10.1007/s13593-014-0280-z.
Miller, D.P., Howell, G.S., Flore, J.A., 1997. Influence of shoot number and crop load on potted Chamburcin grapevines: II. Whole-vine vs. single-leaf photosynthesis. Vitis 36, 109–114.
Minasny, B., McBratney, A.B., 2002. FuzzME version 3.0. Univ. Sydney.
Naor, A., Gal, Y., Bravdo, B., 1997. Crop load affects assimilation rate, stomatal conductance, stem water potential and water realtions of field-grown Sauvignon Blanc grapevines. J. Exp. Bot. 48, 1675–1680.
Naschitz, S., Naor, A., 2005. The effect of crop load on tree water consumption of Golden Delicious apples in relation to fruit size: an operative model. J. Am. Soc. Hortic. Sci. 130, 7–11.
Otsu, N., Smith, P.L., Reid, D.B., 1979. A threshold selection method from gray-level histograms. IEEE Trans. Syst. Man Cybern. 9, 62–66.
Pou, A., Diago, M.P., Medrano, H., Baluja, J., Tardaguila, J., 2014. Validation of thermal indices for water status identification in grapevine. Agric. Water Manag. 134, 60–72, http://dx.doi.org/10.1016/j.agwat.2013.11.010.
Reynolds, A.G., Heuvel, J.E.V., 2009. Influence of grapevine training systems on vine growth and fruit composition: a review. Am. J. Enol. Vitic. 60, 251–268.
Santesteban, L.G., Miranda, C., Royo, J.B., 2011. Thinning intensity and water regime affect the impact cluster thinning has on grape quality. Vitis - J. Grapevine Res. 50, 159–165.
Santesteban, L.G., Miranda, C., Urretavizcaya, I., Royo, J.B., 2012. Carbon isotope ratio of whole berries as an estimator of plant water status in grapevine (Vitis vinifera L.) cv Tempranillo. Sci. Hortic. (Amst.) 146, 7–13.
Santesteban, L.G., Guillaume, S., Royo, J.B., Tisseyre, B., 2013. Are precision agriculture tools and methods relevant at the whole-vineyard scale? Precis. Agric. 14, 2–17, http://dx.doi.org/10.1007/s11119-012-9268-3.
Santesteban, L.G., Miranda, C., Barbarin, I., Royo, J.B., 2015. Application of the measurement of the natural abundance of stable isotopes in viticulture: a review. Aust. J. Grape Wine Res. 21, 157–167, http://dx.doi.org/10.1111/ajgw.12124.
Santos, A.O., Wample, R.L., Sachidhanantham, S., Kaye, O., 2012. Grape quality mapping for vineyard differential harvesting. Braz. Arch. Biol. Technol. 55, 193–204.
Sepulcre-Canto, G., Zarco-Tejada, P.J., Jimenez-Munoz, J.C., Sobrino, J.A., de Miguel, E., Villalobos, F.J., 2006. Detection of water stress in an olive orchard with thermal remote sensing imagery. Agric. For. Meteorol. 136, 31–44.
Serrano, J., da Silva, J.M., Shahidian, S., Silva, L., Sousa, A., Baptista, F., 2015. Spatial variability of soil phosphorus, potassium and pH: evaluation of the potential for improving vineyard fertilizer management. In: Precision Agriculture '15. Wageningen Academic Publishers, The Netherlands, pp. 495–502, http://dx.doi.org/10.3920/978-90-8686-814-8_61.
Taylor, J.A., Acevedo-Opazo, C., Ojeda, H., Tisseyre, B., 2010. Identification and significance of sources of spatial variation in grapevine water status. Aust. J. Grape Wine Res. 16, 218–226, http://dx.doi.org/10.1111/j.1755-0238.2009.00066.x.
Testi, L., Goldhamer, D.A., Iniesta, F., Salinas, M., 2008. Crop water stress index is a sensitive water stress indicator in pistachio trees. Irrig. Sci. 26, 395–405, http://dx.doi.org/10.1007/s00271-008-0104-5.
Urretavizcaya, I., Santesteban, L.G., Tisseyre, B., Guillaume, S., Miranda, C., Royo, J.B., 2014. Oenological significance of vineyard management zones delineated using early grape sampling. Precis. Agric. 15, 111–129, http://dx.doi.org/10.1007/s11119-013-9328-3.
Urretavizcaya, I., Royo, J.B., Miranda, C., Tisseyre, B., Guillaume, S., Santesteban, L.G., 2016. Relevance of sink-size estimation for within-field zone delineation in vineyards. Precis. Agric., 1–12, http://dx.doi.org/10.1007/s11119-016-9450-0.
Viguié, V., Lecocq, F., Touzard, J.-M., 2014. Viticulture and adaptation to climate change. J. Int. des Sci. la Vigne du Vin, 55–60.
Yuan, B.Z., Sun, J., Nishiyama, S., 2004. Effect of drip irrigation on strawberry growth and yield inside a plastic greenhouse. Biosyst. Eng. 87, 237–245, http://dx.doi.org/10.1016/j.biosystemseng.2003.10.014.
Zarco-Tejada, P.J., González-Dugo, V., Berni, J.A.J., 2012. Fluorescence, temperature and narrow-band indices acquired from a UAV platform for water stress detection using a micro-hyperspectral imager and a thermal camera. Remote Sens. Environ. 117, 322–337, http://dx.doi.org/10.1016/j.rse.2011.10.007.